Showcasing research from Professor Claire Villevieille, LEPMI, UGA Grenoble, France and Professor Hubert Girault, ISIC, EPFL Lausanne, Switzerland.

Redox aspects of lithium-ion batteries. Is graphite an anode?

This paper examines the potential-dependent intercalation steps of lithium cations into graphite from an electrochemical perspective. In the absence of redox reactions, it is argued that a graphite negative electrode cannot strictly be classified as an anode. The message (in the bottle...) behind this picture is that graphite is not an electrode where electrochemical reactions take place, but a volumic capacitor called here a capacitive rack, where ions are stored like wine bottles in a wine rack. It illustrates that a lithium battery with a graphite electrode is a mixed redox/capacitor energy storage device, with electrochemical reactions at the positive electrode and electrostatic charging at the negative electrode.

Image reproduced by permission of Claire Villevieille from *EES Batteries*, 2026, **2**, 103.

As featured in:

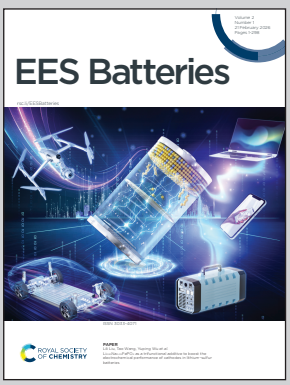

See Hubert Girault *et al.*, *EES Batteries*, 2026, **2**, 103.

ROYAL SOCIETY OF CHEMISTRY

rsc.li/EESBatteries

Registered charity number: 207890

EES Batteries

PERSPECTIVE

View Article Online
View Journal | View Issue

Cite this: *EES Batteries*, 2026, **2**, 103

Redox aspects of lithium-ion batteries. Is graphite an anode?

Corentin Renais, [a] Claire Villevieille, [a] Pekka Peljo, [b] Fatima El Bachraoui [c] and Hubert Girault *[c,d]

Received 20th October 2025,
Accepted 28th October 2025

DOI: 10.1039/d5eb00202h

rsc.li/EESBatteries

Graphite is the most commonly used negative electrode in lithium-ion batteries. This perspective article reviews the charge transfer aspects of the graphite electrode, presenting the different mechanisms of the graphite electrode involved during its charging from an electrochemical standpoint. Different reaction mechanisms can be distinguished: (1) adsorption of solvated lithium ions on negatively charged graphite, (2) intercalation of de-solvated lithium ions in graphite as a solid solution, (3) biphasic (liquid–solid) formation of solid LiC_{36} and LiC_{12} phases, (4) biphasic (solid–solid) formation of a LiC_6 phase and (5) under potential deposition of lithium atoms on the LiC_6 phase, which may be followed by classical electroplating of Li^+ on Li. Only the last electrodeposition reactions are truly a redox process. The other reaction mechanisms represent the potentiometric titration of carbon sites for lithium ion adsorption and intercalation.

Broader context

As global efforts intensify to advance energy storage for decarbonized transport and grid resilience, lithium-ion batteries remain at the forefront due to their high energy density and scalability. Graphite, the dominant negative electrode material, has been central to their success, yet its fundamental electrochemical behavior is often oversimplified. This article revisits graphite's role from a mechanistic and thermodynamic standpoint, challenging its traditional classification as an anode. By dissecting the sequence of lithium insertion processes—from surface adsorption to underpotential deposition—the authors reveal that most stages lack true redox character. This nuanced understanding reshapes how graphite is conceptualized in battery science and underscores the need for precise definitions in developing next-generation storage materials.

1. Introduction

Li-ion batteries are currently the most advanced electrochemical energy storage systems, essential for both stationary storage and e-mobility.

In a previous communication, we have addressed the redox reactions at the positive electrode[1] and discussed the electrochemical aspects of the so-called "cathode material". Here, we shall discuss from an electrochemical viewpoint the charge transfer reactions taking place at the negative electrode.

Graphite negative electrodes remain the most widely commercialised material due to their excellent electrochemical properties. As an electroactive material, graphite offers a low working potential (close to that of lithium metal), is cost-effective and environmentally friendly, and delivers a reasonable specific charge (372 mAh g^{-1}) over a large number of cycles.

This longevity is primarily attributed to a specific surface reaction known as the solid electrolyte interphase (SEI), which forms during the initial cycle and protects the graphite from further electrolyte decomposition. Although the SEI is advantageous for graphite in today's commercial systems, it presents challenges for other high-energy-density technologies, such as the 5 V positive electrode. In these systems, transition metal leaching at high potential migrates to the SEI layer, initiating nucleation and rendering the SEI unstable, ultimately leading to poor electrochemical performance.

Similarly, alternative electroactive materials like silicon have demonstrated the ability to deliver exceptionally high specific capacity, up to ten times that of graphite. However, their alloying process, combined with a low potential and significant volume changes during cycling, results in unstable SEI formation, which has hindered their commercialisation so far.

Despite years of intensive research, graphite continues to pose challenges for the development of next-generation Li-ion batteries. These challenges stem from its complex reaction

[a]*Univ. Grenoble Alpes, Univ. Savoie Mont Blanc, CNRS, Grenoble INP, LEPMI, Grenoble, France*
[b]*Department of Chemistry and Materials Science, Aalto University, P.O. Box 16100 Aalto, Espoo, 00076 Finland*
[c]*Material Science, Energy and Nanoengineering (MSN) department, University Mohammed VI Polytechnic, 43 150 Ben Guerir, Morocco.*
E-mail: hubert.girault at epfl.ch
[d]*Institute of Chemical Science and Engineering, Station 6, Ecole Polytechnique Federale de Lausanne, CH-1015 Lausanne, Switzerland*

mechanisms, multiple phase transitions during cycling, and unclear solid-state charge transport processes, that hinder high-power applications.

Nevertheless, the graphite negative electrode remains the most commercially viable option. To enhance its specific charge, graphite is currently combined with silicon nanomaterials to increase its specific energy. However, an excessive amount of silicon results in poor long-term electrochemical performance.

In a previous communication, we explored the redox aspects of lithium-ion batteries, focusing on the metal oxide redox solids present at the positive electrode. Here, we will examine the electrochemical reactions occurring within the graphite negative electrode and ask whether it is, strictly speaking, an 'anode'.

2. Graphite charging stages

The graphite electrode is indeed a major component of most lithium ion-batteries. It has been thoroughly discussed and reviewed.[2] Nonetheless, it remains a topic of active research both theoretically and experimentally, particularly using *in operando* techniques. Graphite lithiation is usually described by the Daumas–Herold[3] or Rüdorff–Hofman[4] nomenclatures, which categorise the different lithiation stages based on the number of graphite layers separating the lithium cation layers.

In the so-called dilute stages, lithium is sparsely distributed, and these stages are described as 'liquid-like' (often denoted by 'L' to indicate the liquid-like phase). In contrast, during the dense stages, lithium layers become ordered, adopting a 'solid-like' structure.

Starting from the fully lithiated LiC_6 phase, the different stages are as follows:

- **Stage 1**, the more densely packed and fully lithiated graphite, is a LiC_6 phase, which has a theoretical specific capacity of 372 mAh g^{-1},
- **Stage 2** is also a pure solid phase in which fully lithiated layers are separated by two graphite layers. It can be described as a LiC_{12} phase.
- **Stage 2-L** is a solid solution in which no in-plane order is observed.
- **Stages 3, 4** are solid phases and are characterised by lithiated layers separated by 3 and 4 graphite layers, respectively. Stage 4 can be described as LiC_{36} phase.
- **Stage 1-L** is a solid solution with every interlayer filled with lithium ions but in a diluted manner, as a diluted stage 1. No in-plane order is observed.
- **Stage P** is the pristine graphite form.

The different lithiation stages are illustrated in Fig. 1a, which presents the galvanostatic curve of a graphite electrode cycled against a lithium metal electrode, which serves as both the reference and the counter electrode. As such, this graph represents a potentiometric titration curve of the different intercalation sites.

The graphite lithiation profile exhibits distinct features in terms of potential evolution, which have been extensively described since the 1990s. Three primary potential plateaus are observed, corresponding to x = [0.08–0.16], [0.25–0.52] and [0.52–0.95] (±0.01), note that stage II is observed for $x \approx 0.52$ and not for 0.5. This difference comes from the adsorbed charges and the charges involved in the SEI that are considered in the overall electronic charge (x), slightly increasing the specific capacity of graphite. The associated phase transitions are indicated at the top of Fig. 1a.

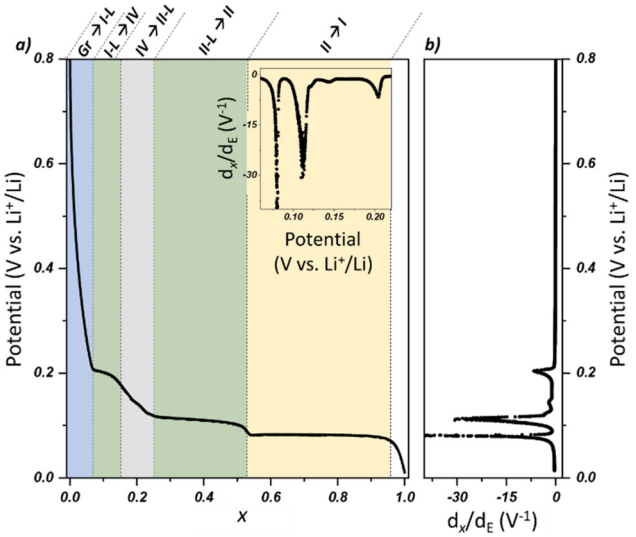

Fig. 1 (a) Voltage profile for constant-current cycling of a Li|graphite half-cell (*vs.* Li metal) between 1.2 V–0.01 V and representation of the different stages of graphite lithiation, where x represents the proportion of the overall electronic charge that can be stored. [Adapted from ref. 5]; (b) the corresponding differential curves showing the different graphite stages.

Differential capacity analysis (DCA), as shown in the inset of Fig. 1a and in Fig. 1b, provides valuable information on the lithium intercalation mechanism.

For instance, it is widely recognised that a solid–solid biphasic state occurs within the range x = 0.52–0.95 (yellow zone), where LiC_6 phases (stage I) progressively form from LiC_{12} phases (stage II). This solid–solid biphasic mechanism, observed in various insertion materials such as $LiFePO_4$, is characterised by the coexistence of two pure solid phases with constant chemical potentials, meaning that the composition of each phase remains unchanged, only their volume is changing. In such a first-order transition, the cell voltage is expected to be constant because of the coexistence of two pure phases. Consequently, a divergence of d_x/d_E should be observed in DCA.[6,7] Experimentally, within the yellow zone (Fig. 1a), the potential evolution remains remarkably flat, and the corresponding DVA peak is narrow. However, kinetic effects induce a slight potential decrease, preventing a true divergence. In contrast, within the green zones attributed to "solid solution-solid" reactions (as discussed below), the potential evolution is more pronounced, and larger peaks appear in the DVA representation. The distinction between the green and yellow zones underscores the differences in lithium

intercalation reaction mechanisms, *i.e.* solid solution-solid and solid–solid, which are responsible for differences in potential evolution—a topic further explored in the following sections.

3. Graphite charging – electrochemical modelling

To electrochemically model the charging process of a graphite electrode, we must consider several key steps. The first involves the adsorption of solvated lithium cations onto the graphite surface. Next, these cations undergo desolvation and intercalation, becoming sparsely distributed across certain layers—lacking true structural order apart from a superstructure before condensing into specific phases.

To distinguish these different steps, we will consider an electrochemical cell model comprising a pristine graphite electrode (G) and a lithium metal electrode, separated by an electrolyte solution (S) containing a lithium salt (Li^+A^-) as given by **Cell I.**

Cell I:

$$M^I|\text{lithium metal (Li)}|\text{lithium electrolyte (S)}|\text{graphite (G)}|M^{II}$$

The cell voltage, which can be measured experimentally using a simple voltmeter, is defined as the Galvani potential difference between the two current collectors (M^I and M^{II}) made of the same metal and inert *vs.* Li and connected to the graphite and lithium electrodes, respectively. The cell voltage is expressed in eqn (1):

$$\begin{aligned}[E]_{vs.\,Li^+/Li} &= \phi^{M^{II}} - \phi^{M^I} \\ &= (\phi^{M^{II}} - \phi^{G}) + (\phi^{G} - \phi^{S}) + (\phi^{S} - \phi^{Li}) + (\phi^{Li} - \phi^{M^I})\end{aligned} \quad (1)$$

where ϕ represents the Galvani potential, also called the inner potential of the different phases in contact. To proceed, we must define the electrochemical potential of the electron as the energy required to bring an electron from vacuum into a given phase, which is expressed by eqn (2).[8]

$$\tilde{\mu}_{e^-} = \mu_{e^-} - F\chi - F\psi = \mu_{e^-} - F\phi = -\Phi - F\psi \quad (2)$$

where μ_{e^-} represents the chemical potential of the electron, χ the surface potential of the phase and ψ the outer potential of the phase associated to the presence of an excess charge on its surface. Φ represents the work function, the work to extract an electron from an uncharged phase. Φ defines the Fermi level of the electron in the phase with respect to vacuum. At the M^{II}|graphite junction, electrons can move freely, leading to equalization of the electrochemical potential of the electron in both M^{II} and graphite, as expressed in eqn (3):

$$\phi^{M^{II}} - \phi^{G} = (\mu_{e^-}^{M^{II}} - \mu_{e^-}^{G})/F. \quad (3)$$

At the lithium counter/reference electrode, the Galvani potential difference between the lithium metal and the electrolyte solution (S) is given by considering the electrochemical redox equilibrium (reaction (I)):

$$Li^{+S} + e^{-Li} \rightleftarrows Li. \quad (I)$$

At equilibrium, the electrochemical potentials of the reactants and the products are equal (eqn (4)):

$$\mu_{Li} = \tilde{\mu}_{Li^+}^{S} + \tilde{\mu}_{e^-}^{Li} \quad (4)$$

where μ_{Li} represents the work that is done to add an atom of lithium to a pure lithium metal phase. By developing the electrochemical potential of an ionic species as follows (eqn (5)):

$$\tilde{\mu}_i = \mu_i + z_i F\phi = \mu_i^{o} + RT\ \ln\ a_i + z_i F\phi \quad (5)$$

the Galvani potential difference between the lithium metal and the electrolyte solution is given by (eqn (6)):

$$\phi^{S} - \phi^{Li} = (\mu_{Li} - \mu_{Li^+}^{o,S} - \mu_{e^-}^{Li})/F - \frac{RT}{F}\ln\ a_{Li^+}^{S} \quad (6)$$

$\mu_{Li^+}^{o,S}$ represents the work to bring a lithium cation from vacuum to the electrolyte solution under standard conditions (*e.g.* 1 M), which is also the standard solvation energy, as illustrated below in Fig. 2.

As shown by (eqn (2)), $-\mu_{e^-}^{Li}$ represents the work to extract an electron from the Fermi level of a neutral lithium metal, *i.e.* the work function of lithium (about 3.1 eV (ref. 9)) and where a is the activity of the lithium ion in the electrolyte solution; the activity of lithium in the metallic phase is unity as it is a pure metal. μ_{Li} can be approximated as being minus the energy of sublimation of lithium, *i.e.* 159 kJ mol^{-1} (Wikipedia). To give an order of magnitude, the Gibbs solvation of Li^+ in propylene carbonate solution was calculated to be around −540 kJ mol^{-1}.[10]

At the M^I|lithium metal junction, electrons move freely, leading to the equalisation of the electrochemical potential of the electron in both the lithium metal and M^I, as expressed in eqn (7)

$$\phi^{Li} - \phi^{M^I} = (\mu_{e^-}^{Li} - \mu_{e^-}^{M^I})/F. \quad (7)$$

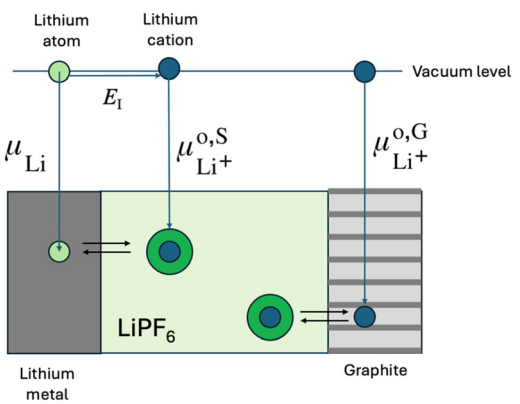

Fig. 2 Thermodynamic cycle for lithium cation insertion in graphite, where E_I is the ionisation energy of a lithium atom. The green central zone represents the electrolyte solution.

Consequently, eqn (1) simplifies to

$$[\mathrm{E}]_{vs.\ \mathrm{Li^+/Li}} = \phi^{\mathrm{M^{II}}} - \phi^{\mathrm{M^I}} = (\phi^{\mathrm{G}} - \phi^{\mathrm{S}}) + (\mu_{\mathrm{Li}} - \mu^{\mathrm{o,S}}_{\mathrm{Li^+}} - \mu^{\mathrm{G}}_{\mathrm{e^-}})/F - \frac{RT}{F}\ln\, a^{\mathrm{S}}_{\mathrm{Li^+}}. \quad (8)$$

With this foundation established, we can now examine the graphite|electrolyte solution interface to express the first term of eqn (8).

3.1. Lithium adsorption on graphite

In the initial step of charging a pristine graphite particle, the electrode reaction can be defined as a simple electro-adsorption process of a solvated lithium ion on an inert electrode, as illustrated in Fig. 3a and expressed by reaction (II).

$$\mathrm{Li^{+,S}} \rightleftarrows \mathrm{Li^+_{ads}}. \quad (\mathrm{II})$$

If in a first approximation we ignore the presence of surface groups such as oxides and the presence of the SEI, this is a purely capacitive process in which the outer potential of the graphite varies and the Fermi level of the electrons in graphite rises as the electrode becomes more electronegative. A Frumkin-type approach can be applied to calculate the potential difference in the electrolyte solution between the graphite surface and the bulk electrolyte.

Starting with the equalisation of the electrochemical potential of lithium ions between the bulk electrolyte solution and the graphite surface, we obtain eqn (9):

$$\mu^{\mathrm{o,S}}_{\mathrm{Li^+}} + RT\ln a^{\mathrm{S}}_{\mathrm{Li^+}} + F\phi^{\mathrm{S}} = \mu^{\mathrm{o,S}}_{\mathrm{Li^+}} + RT\ln a^{\mathrm{ads}}_{\mathrm{Li^+}} + F\phi^{\mathrm{ads}}. \quad (9)$$

Therefore, the Galvani potential difference between the solution and the adsorption plane is described by eqn (10).

$$\phi^{\mathrm{ads}} - \phi^{\mathrm{S}} = \frac{RT}{F}\ln\left(\frac{a^{\mathrm{S}}_{\mathrm{Li^+}}}{a^{\mathrm{ads}}_{\mathrm{Li^+}}}\right) \quad (10)$$

where ϕ^{ads} represents the potential in the solution on the surface of the graphite electrode, where solvated lithium ions adsorb. The inner potential of the graphite particle phase varies with changes in the outer potential upon charging.

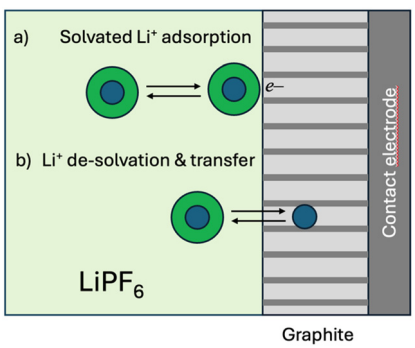

Fig. 3 (a) Schematic representation of the adsorption of a solvated lithium cation on the negatively charged surface of graphite. (b) Schematic transfer of a lithium cation from the electrolyte solution, where it exists in a solvated state, to graphite, where it becomes a bare cation. By definition, the partially lithiated graphite phase remains electrically neutral overall as a result of the electrical charging of the graphite.

The polarised interface can be treated as a capacitor. For an ideally spherical graphite particle with radius R, the potential difference between the graphite and the adsorbed lithium layer is expressed by eqn (11):

$$\phi^{\mathrm{G}} - \phi^{\mathrm{ads}} = Q/C \quad (11)$$

where the capacitance C can be written in a first approximation as in eqn (12):

$$C = 4\pi\varepsilon R^2/\delta \quad (12)$$

where δ is the distance between the adsorbed solvated lithium ions and the graphite edge and ε the permittivity of this layer.

The Frumkin adsorption isotherm expresses the surface coverage θ of the adsorbate to the bulk concentration c and can be expressed as in eqn (13):

$$\theta = \frac{Kc}{1+Kc}\exp^{-a\theta} \quad (13)$$

where K is the adsorption equilibrium constant and a is the parameter representing the interactions between the adsorbed ions. The limiting form at low coverage reads simply (eqn (14)):

$$\theta = Kc. \quad (14)$$

So, the charge of the particle is given by eqn (15):

$$Q = \theta_{\mathrm{Li^+}} Q_{\max} = 4\pi\varepsilon R^2 \theta_{\mathrm{Li^+}} \sigma_{\max}. \quad (15)$$

By substitution, we have eqn (16):

$$\phi^{\mathrm{G}} - \phi^{\mathrm{ads}} = \theta_{\mathrm{Li^+}}\sigma_{\max}/\varepsilon_0. \quad (16)$$

All in all, the cell voltage of **Cell I** is given by eqn (8) and can then be translated into eqn (17):

$$[\mathrm{E}]_{\mathrm{Li^+/Li}} = \phi^{\mathrm{M^{II}}} - \phi^{\mathrm{M^I}} = \theta_{\mathrm{Li^+}}\sigma_{\max}/\varepsilon_0 + (\mu_{\mathrm{Li}} - \mu^{\mathrm{o,S}}_{\mathrm{Li^+}} - \mu^{\mathrm{G}}_{\mathrm{e^-}})/F - \frac{RT}{F}\ln\, a^{\mathrm{ads}}_{\mathrm{Li^+}}. \quad (17)$$

The dominant term in eqn (17) is the last one, which shows that the potential decreases sharply as adsorption progresses as observed at the start of the blue area in Fig. 1a. As expected from adsorption processes on highly ordered materials, the amount of charge stored is relatively small, unless the materials are mesoporous. This simplified approach does not account for the formation of the SEI or surface chemistry effects, such as adventitious carbon.

The final value of x at the end of the surface adsorption step, as shown in Fig. 1a, depends on several factors: (i) the structural order of the material—if the graphite possesses disordered domains (such as in hard carbons), the adsorption process can be more extensive. (ii) The surface roughness—a higher exposed surface area leads to increased adsorption. (iii) The surface chemistry of graphite.

Typically, in conventional graphite electrodes, the adsorption process occurs for small values of x.

3.2. Lithium insertion in graphite – ion transfer reactions

As discussed in the following, during the charging process, solid solutions of lithium ions in graphite are observed. Thermodynamically, a solid solution is characterised by a temperature dependence of the structure,[11] here solid solution means that some lithium ions are free to move in the graphite as in a solvent.

When the graphite presents a solid solution mechanism, lithium ions of the electrolyte solution undergo desolvation, and the bare lithium cation randomly intercalates between graphite sheets, as illustrated in Fig. 3b and expressed in reaction (III).

$$Li^{+,S} \rightleftarrows Li^{+,G}. \quad \text{(III)}$$

Ion transfer reactions have been extensively studied at ITIES (interface between two immiscible electrolyte solutions) for more than a century. These reactions are, in essence, electrochemical reactions, as they are controlled by an applied potential difference between the two phases.

Here, at the electrolyte solution|graphite interface, the equality of the electrochemical potentials reads as in eqn (18):

$$\mu^{o,S}_{Li^+} + RT\ln a^{S}_{Li^+} + F\phi^{S} = \mu^{o,G}_{Li^+} + RT\ln a^{G}_{Li^+} + F\phi^{G}. \quad (18)$$

The negatively charged graphite acts as a "solvent" for lithium cations. From eqn (18), we can derive the Nernst equation for the lithium ion transfer[7] reaction as given by eqn (19).

$$\phi^{G} - \phi^{S} = (\mu^{o,S}_{Li^+} - \mu^{o,G}_{Li^+})/F + \frac{RT}{F}\ln\left(\frac{a^{S}_{Li^+}}{a^{G}_{Li^+}}\right) \quad (19)$$

$\mu^{o,S}_{Li^+}$ and $\mu^{o,G}_{Li^+}$ are illustrated in Fig. 2 and represent the standard solvation energy of the lithium cation in its respective standard states. For the electrolyte solution, the standard state is typically defined by a concentration of 1 M, while for the solid solution graphite phase, it corresponds to a molar fraction of unity—*i.e.* a hypothetical fully charged 'solid solution' graphite.

During the charge of the solid solution, the graphite electrode functions neither as a cathode nor as an anode, as no redox reactions occur. Instead, it operates as a porous electrode, charging *via* ion transfer/insertion under the applied potential and subsequently releasing charge through ion extrusion.

The key distinction from the simple solvated lithium cation adsorption described earlier in eqn (17) lies in the desolvation/resolvation reaction occurring during insertion/extraction. Based on eqn (8) and (19), the voltage of **Cell I** is then given by eqn (20).

$$[E]_{vs.\,Li^+/Li} = (\mu_{Li} - \mu^{o,G}_{Li^+} - \mu^{G}_{e^-})/F - \frac{RT}{F}\ln a^{G}_{Li^+}. \quad (20)$$

This potential difference is independent of the lithium concentration in the electrolyte. Eqn (20) is the "Master equation" expressing the potential dependence upon charging when some solid solution phases are present. It shows why the potential decreases upon lithium-ion insertion. $\mu^{o,G}_{Li^+}$ can then be estimated from eqn (20) using the thermodynamic cycle of Fig. 2 with the following values:

- 160 kJ mol^{-1} (sublimation energy of lithium),
- 450 kJ mol^{-1} (estimated work function of graphite),
- 200 kJ mol^{-1} (experimental cell voltage at 0.2 V for the blue and grey zone taken as a first average approximation)

This yields an approximate value of −810 kJ mol^{-1}, suggesting that graphite serves as a more effective 'solvent' for bare lithium cations compared to propylene carbonate (−540 kJ mol^{-1}).

The dissolution of bare lithium cations in graphite, being an ion transfer reaction, allows graphite to be considered an "ionode", using the terminology proposed for ion transfer reactions at liquid|gel interfaces[12] Here, the ion transfer reaction occurs between an organic liquid electrolyte solution and a graphite phase exhibiting a "liquid-like" behaviour.

3.3. Lithium insertion in graphite-biphasic system: "solid solution – solid" regions

In the blue zone (Fig. 1a), the adsorbed lithium ions start to de-solvate and intercalate in the graphite. Experimental studies have shown that lithium can begin to intercalate into the graphite structure at potentials below 0.5 V *vs.* Li$^+$/Li.[13] When entering the first green zone at x = 0.08, the process is still being discussed in the literature about the nature of the Li_xC_6 compound. Based on Dahn's work in 1991,[11] this intermediate is a diluted stage I, displaying no in-plane order with intercalants in every graphite interlayer. Following this hypothesis, some authors consider this phase as a solid solution.[14,15] On the other hand, some consider this intermediate to be an 8th stage with lithium intercalant in every 8 graphite layer, supporting a "pure" solid phase.[16–18] Based on the electrochemical profile from x = 0.08 to 0.16, the hypothesis of a solid solution (stage 1-L) is preferred here as explained below.

Upon further insertion of lithium ions in the remaining free graphite, the lithium ions are mobile in a solid solution phase and a stage IV starts to form, or so to speak to precipitate to form LiC_{36}.[18]

Similarly, at the end of grey zone, where the potential also varies rather strongly, the lithium ions are mobile in a solid solution stage II-L and a stage II starts to form.

In the two green zones (Fig. 1a), the randomly distributed lithium ions in the solid solution "precipitate" to form a solid LiC_{36} [18] and LiC_{12} phase, respectively. From a thermodynamic perspective, the reaction can be stoichiometrically expressed as reactions (IV) and (V):

$$Li^{+,S} + e^{-G} + 36\ C^{G} \rightleftarrows [Li^{+}C_{36}{}^{-}]^{LiC_{36}} \quad \text{(IV)}$$

$$Li^{+,S} + e^{-G} + 12\ C^{G} \rightleftarrows [Li^{+\delta}C_{12}{}^{-\delta}]^{LiC_{12}} \quad \text{(V)}$$

where the reactants are a solvated lithium ion in the electrolyte solution, an electron from the graphite and 36 or 12 carbon atoms from the graphite structure, respectively.

In the case of LiC_{36}, the concentration of lithium in graphite is small enough to consider that the cation conserves its positive charge.

In the case of LiC_{12}, there are two limiting situations to consider: either as an ionic solid $Li^+C_{12}^-$ ($\delta = 1$) or simply as a neutral solid ($\delta = 0$). It is important to note that the Li–C interaction is probably partially ionic with ($0 < \delta < 1$), but this falls beyond the scope of the present discussion. Regardless of the specific nature of the interaction, the phase remains globally neutral.

Reactions (IV) and (V) may appear to be a reduction reaction of the lithium cation, but in fact, they correspond to the formation of a neutral phase. For LiC_{12}, it can be interpreted as a partial reduction of Li^+, where $0 < \delta < 1$. In this framework, graphite could be partially considered as an anode, although this interpretation extends beyond the strict IUPAC definition.[19]

From the perspective of electrochemical potentials, we can ascribe LiC_{36} and LiC_{12} as a homogeneous phase and write eqn (21) and (22).

$$(\mu^{o,S}_{Li^+} + RT\ln a^S_{Li^+} + F\phi^S) + (\mu^G_{e^-} - F\phi^G) + 36\mu^G_C = \mu_{LiC_{36}} \quad (21)$$

$$(\mu^{o,S}_{Li^+} + RT\ln a^S_{Li^+} + F\phi^S) + (\mu^G_{e^-} - F\phi^G) + 12\mu^G_C = \mu_{LiC_{12}}. \quad (22)$$

From which, using eqn (8), we obtain the following equation (eqn. (23) and (24)) for the end of the green zones ($x = 0.16$ & $x = 0.52$ in Fig. 1a).

$$[E]_{vs.\ Li^+/Li} = (\mu_{Li} - \mu_{LiC_{36}} + 36\mu^H_C)/F \quad (23)$$

$$[E]_{vs.\ Li^+/Li} = (\mu_{Li} - \mu_{LiC_{12}} + 12\mu^H_C)/F \quad (24)$$

Eqn (23) and (24) represents the equilibrium potential of homogeneous solid LiC_{36} & LiC_{12} electrodes immersed in a lithium electrolyte solution, measured against a lithium metal counter electrode, as shown in **Cell II**.

Cell II:

$$M^I|\text{lithium metal}|\text{lithium electrolyte solution}|LiC_{36/12}|M^{II}$$

To calculate the potential in the green zones ($0.08 < x < 0.16$ and $25 < x < 0.52$, Fig. 1a), eqn (20) applies as we are partially in the presence of a solid solution phase, and we can draw an analogy with the potentiometric titration of silver cations in aqueous solutions, by adding KBr. In this widely used potentiometric titration, the potential of a silver electrode immersed in the electrolyte solution is governed by the Nernst equation of the Ag^+/Ag couple. Upon addition of the titrant solution, AgBr begins to precipitate, leading to a decrease of the concentration of Ag^+ concentration to its minimum value, determined by the solubility product, K_S, of AgBr, such that $[Ag^+]_{min} = (K_S)^{1/2}$, thus marking the endpoint of the reaction.

In the present case, we 'titrate' C_6 sites by introducing Li^+ and electrons, and we can consider the 'precipitation' of LiC_{36} or LiC_{12} solids. The potential of **Cell I** remains governed by eqn (20) since part of the phase persists as a solid solution, and the potential varies as the concentration of free lithium ions in the solid solution increases as the volume of the solid solution decreases due to the formation of the solid phases. The electric charge x in Fig. 1a associated to inserted lithium ions in the graphite is no longer solely determined by the molar fraction of freely moving Li^+ within the film—it also includes the fraction of 'precipitated' Li^+, forming the LiC_{36} & LiC_{12} phases.

The variation in potential within the green zones (Fig. 1a), based on this redox titration approach, is further developed in the SI (see eqn (S6)).

At $x = 0.52$, where the potential is defined by eqn (24), the material consists of a pure solid phase of LiC_{12}, as schematically illustrated in Fig. 4.

3.4. Lithium insertion in graphite- "biphasic system: solid–solid" region

Upon further charging, we have the following reaction (VI):

$$Li^{+,S} + e^{-G} + LiC_{12} \rightleftarrows 2LiC_6. \quad (VI)$$

Again, by developing the electrochemical potentials of the different species, we obtain the Galvani potential difference between the electrolyte solution and the graphite (eqn (23))

$$\phi^G - \phi^S = (\mu^{o,S}_{Li^+} + \mu^G_{e^-} + \mu_{LiC_{12}} - 2\mu_{LiC_6})/F + \frac{RT}{F}\ln a^S_{Li^+}. \quad (25)$$

By substituting in eqn (8), we finally show that **Cell I** voltage is constant for $x > 0.52$ as we have two pure solid phases in contact, namely LiC_{12} and LiC_6.

$$[E]_{vs.\ Li^+/Li} = \phi^{M^{II}} - \phi^{M^I} = (\mu_{Li} + \mu_{LiC_{12}} - 2\mu_{LiC_6})/F \quad (26)$$

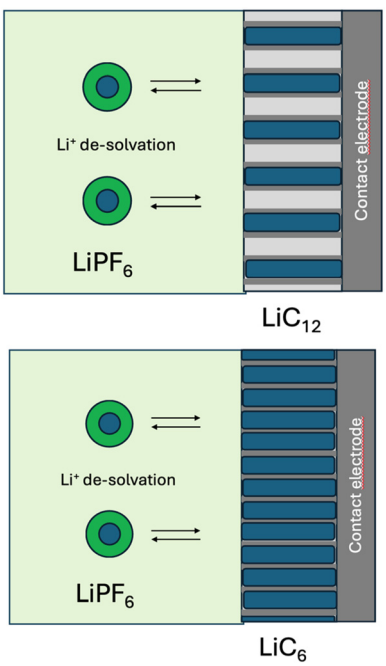

Fig. 4 Schematic reaction between solvated lithium cation and the solid phase LiC_{12} (top) and LiC_6 (bottom). The blue represents the graphite sheets filled to form a solid phase.

Eqn (26) is the equilibrium potential of a LiC_{12}/LiC_6 electrode immersed in a lithium electrolyte solution and measured *versus* a lithium metal counter electrode.

The formation of two pure solid phases LiC_{12} and LiC_6 explained the flat voltage profile in Fig. 1 for $x > 0.52$. The phases LiC_{12} and LiC_6 have a strong metallic character, as illustrated by the golden and reflective colour of LiC_6 as reported, for example, by Gao *et al.*[20]

It is interesting to note that from an electrochemical viewpoint, the potential response does not depend on the electronic structure of the pure phases.

It is independent of the fact that the lithium cations are partially reduced, *i.e.*, that electrons "visit" the 2s orbital of the bare lithium ions and hence contribute to the definition of the Fermi level.

3.5. Lithium metal deposition on LiC_6

Finally, once the graphite electrode is nearly fully lithiated ($x = 0.95$), we can observe lithium metal under potential deposition on the surface of the LiC_6 electrode at a potential of +80 mV. Under potential metal deposition (UPMD) has been studied for decades. It corresponds to the deposition of a monolayer of metal atoms "A" onto another metal substrate "B", at potentials more positive than the reversible Nernst potential of the deposition of metal "A" on "A", for example, as given by eqn (I). In 1974, Kolb *et al.*[21] had shown that the underpotential difference was proportional to the difference in the work functions of metals "A" and "B".

Compared to Cell I for the deposition of lithium on lithium, we have the deposition of lithium on LiC_6 as given by reaction (VI).

$$Li^{+S} + e^{-LiC_6} \rightleftarrows Li_{UPD}. \quad (VI)$$

For which we have

$$\mu_{Li_{UPD}} = \tilde{\mu}^{S}_{Li^+} + \tilde{\mu}^{LiC_6}_{e^-} \quad (27)$$

which can be compared to eqn (4).

At that stage, the system is that given by **Cell III.**

Cell III:

$$M^{I}|\text{Li metal}|\text{lithium electrolyte} \mid Li_{UPD}|LiC_6|M^{II}$$

and is governed by following Nernst equation (similar to eqn (6))

$$\phi^{S} - \phi^{LiC_6} = (\mu_{Li_{UPD}} - \mu^{o,S}_{Li^+} - \mu^{LiC_6}_{e^-})/F - \frac{RT}{F}\ln a^{S}_{Li^+}. \quad (28)$$

By substituting in eqn (8), we finally show that **Cell III** voltage is

$$[E]_{vs.\ Li^+/Li} = \phi^{M^{II}} - \phi^{M^{I}} = (\mu_{Li} - \mu_{Li_{UPD}})/F. \quad (29)$$

Large UPMD favours monolayer deposition and small UPMD favours 3D nucleation. As shown in Fig. 1a, the potential is positive about 80 mV at the start of the UPMD and reaches zero once a lithium metal film or lithium 3D islands start to grow.

4. Discussion and scope

The understanding of graphite as a negative electrode material has been refined through multiple characterisation techniques and modelling, highlighting the nature of the Li–C interaction at the atomic scale, the staging phenomenon occurring upon lithium intercalation at the lattice scale, and the electrodeposition of lithium on graphite particles.

Describing the energy band structure of the LiC_6 lithium-graphite intercalation compound, Holzwarth and Rabii[22] highlighted a remarkable charge transfer between the lithium 2s and graphite π^* orbitals. Although electrons from the Fermi level exhibited a negligible Li 2s character, the covalent nature of the bond was observed in other electronic states. Later, Hazrati *et al.* analysed the $Li_{0.5}C_6$ and LiC_6 intercalation compounds using van der Waals density functional theory (DFT) compared to pristine graphite.[23] Based on phonon densities of states, vibrational modes clearly involve mixed contributions from lithium and carbon, supporting a partial charge transfer between the two entities.

Ultimately, as described by Kganyago and Ngoepe,[24] in lithium-graphite intercalation compounds such as solid-phase LiC_6, electrons from the 2s orbitals of lithium atoms appear partially delocalized onto the π^* orbitals of carbon atoms, with lithium acting as an electron donor. Expanding on this aspect, Insinna *et al.*[25] studied graphite–lithium compounds using electron paramagnetic resonance (EPR). The authors highlighted a greater metallic behaviour for the dense stages compared to that for the diluted ones. The observed *g*-factors correlate the metallic character with the larger contribution of the Li 2s orbital to the Fermi level of graphite, which is responsible for higher conductivities.

At the lattice scale, Weng *et al.*[26] examined the staging structure of graphite both macroscopically (XRD) and microscopically (cryo-TEM), proposing a revised model of lithiation. Their study showed that all stages of lithiated graphite exhibit a long-range order that can be characterised by X-ray or neutron diffraction. This macroscopic order tends to form phase domains, consistent with Daumas–Hérold model. However, each stage of lithiated graphite consists of a mixture of microscopic domains—specifically, stage II is composed of a mixture of stage III and stage I forming domains. This proposed "localised-domains" model is supported by DFT calculations, which highlight the metastable nature of the various lithiation stages. Consequently, disproportionation of stages is more favourable, reinforcing the microscopic observation of domain mixtures.

Gao *et al.* discussed the interplay between lithium intercalation and plating based on *operando* microscopy measurements.[20] Thermodynamically, lithium plating is initiated when the graphite voltage drops around 0 V (*vs.* Li^+/Li). Under kinetic limitations, since lithium solid diffusion within individual graphite particles constrains the system, the authors demonstrated that the sufficient condition to trigger lithium plating is the lithium concentration at the particle surface. If the lithium concentration reaches saturation ($c_s = c_s$, max), lithium plating

becomes more favourable than intercalation. In realistic systems (*i.e.* porous electrodes), the kinetic limitation arises from electrolyte diffusion, making the lithium concentration in the electrolyte solution the critical factor. When lithium depletion is too severe ($c_l \rightarrow 0$), lithium plating is favoured.

Most of the literature is focused on the structural aspects of the graphite lithiation processes. Here, we have focused on the potential-charge relationship. Fig. 1a can be described as a potentiometric titration curve of the different phases. When, the graphite presents some solid solution properties, the Nernst equation for ion transfer reactions (eqn (10)) provides the potential response. When a solid phase starts to precipitate, *e.g.* LiC_{36} or LiC_{12}, this equation is still valid but the concentration of "mobile" lithium ions in the remaining solid solution should be used. When solid phases are present, for $x > 0.5$ the potential is constant as given by eqn (26).

Stricto sensu, neither the adsorption nor the ion transfer reactions are redox reactions, meaning that graphite itself is not an anode. Only the electrodeposition involving the reduction of solvated lithium cations by UPMD or plating is a redox reaction; in this case, the electrode functions as a true anode, but it is composed of the pure "metallic" LiC_6 phase rather than graphite. Otherwise, the graphite electrode operates as a "volumic capacitor".

According to IUPAC,[19] an anode is defined as 'the electrode where oxidation occurs', whereas a cathode is 'the electrode where reduction takes place'. Furthermore, oxidation is formally described as 'the complete removal of one or more electrons from a molecular entity or an increase in the oxidation number of any atom within a substrate', while reduction represents the reverse process.

Thus, from a strict electrochemical perspective, it can be questioned if the negative graphite electrode is truly an anode?

Furthermore, according to the authoritative IUPAC nomenclature, batteries are defined as "devices that store energy to later be converted into electricity using chemical reactions. During discharge of a battery, the anode undergoes an oxidation reaction, which produces electrons, and the cathode undergoes a reduction reaction, which absorbs electrons[27]". According to this definition, if the graphite electrode does not qualify as an anode, the lithium-ion battery is not a battery.

Also, in a previous communication,[1] we argued that the commonly referred "cathode material" is not a cathode, but rather a redox-active particle in solution, with the actual cathode being the carbon black particles.

There is therefore some major discrepancies between the IUPAC definitions consistently used in patent laws, and the terminology used in the many publications and patents on lithium-ion batteries. Perhaps, IUPAC should revise their definitions to avoid further confusion.

5. Conclusions

A thermodynamic approach has been used to define the Nernst equations describing the lithiation of a graphite electrode. The potential charge curve has been treated as a potentiometric titration of the different carbon sites. The different sequential mechanisms involved in this lithiation process can be summarised as follows:

1. Adsorption of solvated lithium onto "negatively" charged graphite corresponding to the start of the blue zone in Fig. 1a.

2. Intercalation or "dissolution" of desolvated bare lithium cations in a "solid solution" exhibiting Nernstian behaviour. The potential varies logarithmically with the concentration of lithium cations "solvated" by graphite and is given by eqn (20). Blue zone and grey zone in Fig. 1a.

3. Formation of a solid LiC_{36} and LiC_{12} phase through a biphasic "solid solution-solid" reaction. The potential remains independent of the lithium concentration in the electrolyte solution, but a logarithmic variation with the Li^+ concentration in the solid solution exists and is given by eqn (S6) (SI). Green zones in Fig. 1a.

4. Formation of a solid LiC_6 phase through a biphasic solid–solid reaction. The potential is also independent of the lithium concentration in the electrolyte solution. Yellow zone in Fig. 1a.

5. Under potential deposition of Li atoms on LiC_6. The last white zone in Fig. 1a, which can be followed by further electroplating.

Another aspect of this work is about the use of the authoritative IUPAC definitions, which are accepted by regulatory bodies.

Indeed, following the electrochemical analysis presented above, it can be questioned if the negative graphite electrode is truly an anode?

Author contributions

The authors all contributed to the elaboration of this electrochemical model of the graphite electrode through many discussions. C. R. & H. G. were responsible for the redaction of the article.

Conflicts of interest

There are no conflicts to declare.

Data availability

No primary research results, software or code have been included and no new data were generated or analysed as part of this perspective.

Supplementary information (SI) is available. Calculation of the potential for the green zone. See DOI: https://doi.org/10.1039/d5eb00202h.

Acknowledgements

The PhD thesis of C. Renais is financed by the Region Auvergne Rhône-Alpes (Pack Ambition Recherche 2021 –

Projet IsoBATT). P. Peljo gratefully acknowledges the funding from the European Research Council (agreement no. 950038).

F. El Bachraoui wishes to thank MSN-UM6P and the Office Chérifien des Phosphates (OCP) for financial support.

References

1 P. Peljo, C. Villevieille and H. H. Girault, *Energy Environ. Sci.*, 2025, **18**, 1658.
2 H. Zhang, Y. Yang, D. Ren, L. Wang and X.- He, *Energy Storage Mater.*, 2021, **36**, 147.
3 N. Daumas and A. Hérold, *CR Acad. Sci. Paris Sér. C*, 1969, **268**, 373.
4 U. Hofmann and W. Rüdorff, *Trans. Faraday Soc.*, 1938, **34**, 1017.
5 C. Renais, M. Mirolo, M. Servajon, J. Drnec, F. Alloin and C. Villevieille, *Chem. Mater.*, 2025, **37**, 5647.
6 W. R. McKinnon, Insertion electrodes I: Atomic and electronic structure of the hosts and their insertion compounds. in *Solid State Electrochemistry*, ed. P. G. Bruce, Cambridge University Press, 1994, pp. 163–198. DOI: 10.1017/CBO9780511524790.008.
7 A. Van Der Ven, J. Bhattacharya and A. A. Belak, *Acc. Chem. Res.*, 2013, **46**, 1216.
8 H. H. Girault, *Electrochimie physique et analytique*, EPFL Press, 2008.
9 S. Trasatti, *J. Chem. Soc., Faraday Trans. 1*, 1972, **68**, 229.
10 M. D. Bhatt, M. Cho and K. Cho, *J. Solid State Electrochem.*, 2012, **16**, 435.
11 J. R. Dahn, *Phys. Rev. B: Condens. Matter Mater. Phys.*, 1991, **44**, 9170.
12 H. J. Lee, C. M. Pereira, A. F. Silva and H. H. Girault, *Anal. Chem.*, 2000, **72**, 5562.
13 C. Sole, N. E. Drewett and L. J. Hardwick, *Faraday Discuss.*, 2014, **172**, 223.
14 C. Didier, W. K. Pang, Z. Guo, S. Schmid and V. K. Peterson, *Chem. Mater.*, 2020, **32**, 2518.
15 C. Schmitt, A. Kube, N. Wagnerand and K. A. Friedrich, *ChemElectroChem*, 2022, **9**, 43.
16 H. Fujimoto, M. Murakami, T. Yamanaka, K. Shimoda, H. Kiuchi, Z. Ogumi and T. Abe, *J. Electrochem. Soc.*, 2021, **168**, 080508.
17 H. Fujimoto, T. Yamaki, K. Shimoda, S. Fujinami, T. Nakatani, G. Kano, M. Kawasaki, Z. Ogumi and T. Abe, *J. Electrochem. Soc.*, 2022, **169**, 070507.
18 S. Takagi, K. Shimoda, J. Haruyama, H. Kiuchi, K. I. Okazaki, T. Fukunaga, Z. Ogumi and T. Abe, *Carbon*, 2023, **215**, 118414.
19 A. D. McNaught and A. Wilkinson, *UAPC: Compendium of Chemical Terminology: The Gold Book*, Blackwell Scientific Publications, Oxford (1997), In-line version (2019) created by S. J. Chalk. ISBN 0-9678550-9-8, 2019, DOI: 10.1351/goldbook.
20 T. Gao, Y. Han, D. Fraggedakis, S. Das, T. Zhou, C. N. Yeh, S. Xu, W. C. Chueh, J. Li and M. Z. Bazant, *Joule*, 2021, **5**, 393.
21 D. M. Kolb, M. Przasnyski and H. Gerischer, *J. Electroanal. Chem. Interfacial Electrochem.*, 1974, **54**, 25.
22 N. A. W. Holzwarth and S. Rabii, *Mater. Sci. Eng.*, 1977, **31**, 195.
23 E. Hazrati, G. A. De Wijs and G. Brocks, *Phys. Rev. B: Condens. Matter Mater. Phys.*, 2014, **90**, 155448.
24 K. R. Kganyago and P. E. Ngoepe, *Phys. Rev. B: Condens. Matter Mater. Phys.*, 2003, **68**, 205111.
25 T. Insinna, E. N. Bassey, K. Märker, A. Collauto, A. L. Barra and C. P. Grey, *Chem. Mater.*, 2023, **35**, 5497–5511.
26 S. Weng, S. Wu, Z. Liu, G. Yang, X. Liu, X. Zhang, C. Zhang, Q. Liu, Y. Huang, Y. Li, M. N. Ateș, D. Su, L. Gu, H. Li, L. Chen, R. Xiao, Z. Wang and X. Wang, *Carbon Energy*, 2023, **5**, e224.
27 https://iupac.org/materialschemistryedu/energy/batteries/.